



RESEARCH PAPER

Static deflection analysis of functionally graded beams using various beam theories

Raghad Azeez Neamah ^{1,†}, Ameen A. Nassar ^{2,†}, Luay S. Alansari ^{1,†},
Emad Kadum Njim ^{3,†}, Lazreg Hadji ^{4,†} and Royal Madan ^{5,*†}

¹Department of Mechanical Engineering, Faculty of Engineering, University of Kufa, Iraq,

²Department of Mechanical Engineering, College of Engineering, University of Basrah, Iraq, ³Ministry of Industry and Minerals, State Company for Rubber and Tires Industries, Najaf, Iraq, ⁴Department of Civil Engineering, University of Tiaret, BP 78 Zaaroura, Tiaret 14000, Algeria, ⁵Department of Mechanical Engineering, Graphic Era (Deemed to be University), Dehradun 248002, Uttarakhand, India

* Corresponding Author

† ragada.deibel@uokufa.edu.iq (Raghad Azeez Neamah); ameen.nasaar@uobasrah.edu.iq (Ameen Ahmed Nassar); luays.alansari@uokufa.edu.iq (Luay S. Alansari); emad.njim@gmail.com (Emad Kadum Njim); lazreg.hadji@univ-tiaret.dz (Lazreg Hadji); royalmadan6293@gmail.com (Royal Madan)

Abstract

In the current study, static deflection analysis of a functionally graded (FG) beam is carried out for various theories such as Euler, Timoshenko, and high-order shear deformation theory. The governing equation was solved using the minimum total potential energy principle. Further, for different types of loads, the static deflection analysis of the FG beam was performed using Navier's solution using the Fortran programming language. Moreover, finite element analysis was also carried out using ANSYS software. In this method, each layer of the FG beam possesses different material properties as per a power law distribution. The different solution techniques are used to calculate the static deflection, and their results are compared. Effect of various parameters such as power index value, modulus ratio, aspect ratio (L/h), and type of loading on the dimensionless transverse deflection of this FG beam model. The results show that the aspect ratio has no significant effect on transverse dimensionless deflection in the case of the Euler beam theory. However, there is a noticeable effect for the Timoshenko and higher-order shear deformation theories, indicating that shear significantly impacts dimensionless transverse deflection for short beams. In addition, it is proven that the present model is reliable and can calculate the static deflection for any other required beam with different loads and dimensions.

Keywords: FG beam; dimensionless transverse deflection; Euler beam theory

AMS 2020 Classification: 37M05; 70C20; 74K10; 74E30

1 Introduction

Recent mechanical and structural applications require improved material properties to meet their requirements, and these applications are creating new mechanical and structural applications. In addition, the mechanical properties of these materials cannot be found in traditional materials like metals, polymers, ceramics, and alloys, nor can they be found in conventional composite materials, such as chopped fiber composites, longitudinal fiber composites, and laminated fiber composites [1–3]. Therefore, advanced materials are used, namely functionally graded materials (FGM), which are materials with a continuously varying composition and microstructure. In addition to exhibiting a gradient of thermal conductivity, strength, and stiffness, FGMs also show a gradient of mechanical properties. Because of their versatility, FGMs are ideal for biomedical engineering, aerospace, and automotive applications [4–8]. Using functionally graded materials (FGM) to achieve the application requirements allows the mechanical properties of the graded structure to be improved [9–13]. In today's materials science and engineering society, functionally graded materials attract tremendous attention as a broad research area [14, 15]. Based on the geometry of the beam, the loading conditions, and the accuracy requirements, the FG beam theory will vary. Euler-Bernoulli theory can be used for FG beams with a thin thickness-to-width ratio or high shear load. In contrast, Timoshenko theory or higher-order shear deformation theories may be required for beams with a high thickness-to-width ratio or those subjected to high shear loads [5, 16]. Several specialized beam theories have been used in the study of FG beams. The results of the studies illustrate the possibility of studying the static deflection of FG beams by using different beam theories with varying degrees of accuracy, depending on the beam theory used. The following are some of the most widely utilized specialized beam theories for FG beams: Higher-order shear deformation theory (HSDT), Peridynamics, Porous beam theory, Viscoelastic beam theory, etc. [17–22]. Certain factors must be considered to determine the correct specialized beam theory for a particular problem. The effects of temperature gradients should be regarded as if, for example, the FG beam is subjected to a temperature gradient. The same applies if the FG beam is porous. In such instances, a theory should incorporate the effect of porosity into the analysis. By using specialized beam theories, it is possible to analyze the behaviour of FG beams under various conditions. It can be argued that specialized beam theories are more accurate and reliable than general beam theories. Many researchers have been presented with multiple specialized analysis methods based on different beam theories to study the static deflection of the FG beam [23–26]. There is much to be gained from these specialized analysis methods about how FG beams behave under load. As a result of them, FG beam analysis and design methods have become more accurate and reliable. However, the complexity and computational requirements of specialized analysis methods can be greater than those of general-purpose analysis methods. Due to computer technology and software advances, specialized analysis methods can now be used more efficiently to study FG beam behaviour [27–29]. The FGMs offer high strength-to-weight ratios along with high-temperature resistance because of various gradation variations such as power law, sigmoid law, exponential law and trigonometric law. Apart from these, the direction of gradation can be unidirectional, bidirectional, and multidirectional [30–33]. Therefore, much research has been carried out in the area of static analysis of beams by employing different methods such as first-order shear deformation theory [34], graded finite element method [35], Iso-geometric analysis [36], etc., to name a few.

The aim of this study is to develop and analyze a model of a supported FG beam based on Euler, Timoshenko, and higher-order shear deformation theories using a new displacement field that differs from previous research. The gradation variation is taken as per the power law variation in the direction of height of the beam, and the rule of mixture is employed to estimate the effective

variation of Young's modulus of elasticity. Such FGMs are easy to fabricate with powder metallurgy and additive manufacturing methods and have demonstrated superior properties compared to those of beams of homogeneous materials. Additionally, a new finite element model for calculating the static deflection of a supported FG beam is constructed using ANSYS software. The static deflection behavior of this new model of supported FG beams under point and distributed loads is studied, considering the effects of the power law index, length-to-height ratio, and modulus ratio. The methodology adopted in this study will benefit industries by solving FG beam problems for various material combinations. It will help optimize designs and understand beam behavior under different loading conditions. The abbreviations used in the paper and their explanations are given in Table 5 in the Nomenclature Section.

2 Simulation methodology

According to the requirements of the mechanical and structural applications, the material properties of the FG beam vary along its thickness or height as per a power law distribution given by Eq. (1).

$$P_z = (P_t - P_b) \left(\frac{z}{h} + \frac{1}{2} \right)^k + P_b, \quad (1)$$

where P_z is the property at any point in the thickness of the FG beam. P_t and P_b are the properties of the top and bottom materials, respectively. h is the thickness of the FG beam. k is the power law index. To estimate the material properties of the composite, a rule of mixture was employed as given by Eq. (2). In addition, P_z can be calculated depending on the volume fraction of the material as follows:

$$P_z = P_t V_t + P_b V_b, \quad (2)$$

where V_b is the volume fraction of bottom material. V_t is the volume fraction of top material, which is computed from the following Eqs. (3)-(4):

$$V_t = \left(\frac{z}{h} + \frac{1}{2} \right)^k, \quad (3)$$

and

$$V_t + V_b = 1. \quad (4)$$

According to Eq. (1), the property at any point in thickness of the FG beam P_z depends on the properties of the two materials (P_t and P_b), the position of the point in thickness, and the material distribution (i.e., the power law index), as shown in Figure 1. This variation in material properties is inconsistent with the assumptions of classical beam theories (the beam is homogeneous along thickness and length directions); therefore, the classical beam theories must be modified to consider the effect of the variation in material properties in the thickness direction.

Suggested analytical model for FGB

Considered an FG beam of length (L) and height (h), which is simply supported. Material properties are varied along the thickness (h) in the z -direction along the (x - z) plane as shown

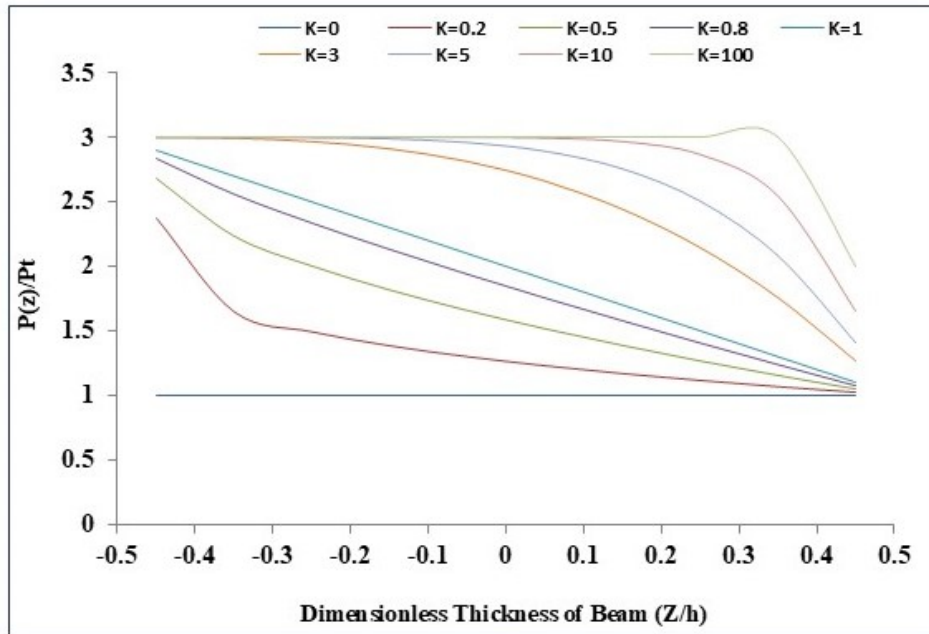


Figure 1. The variation of material property, P_z , along the thickness of the FG beam for different values of power-law index (k) when $P_b/P_t=3$

in **Figure 2.** The deformation of the FG beam in the (X-Z) plane, as well as the displacement

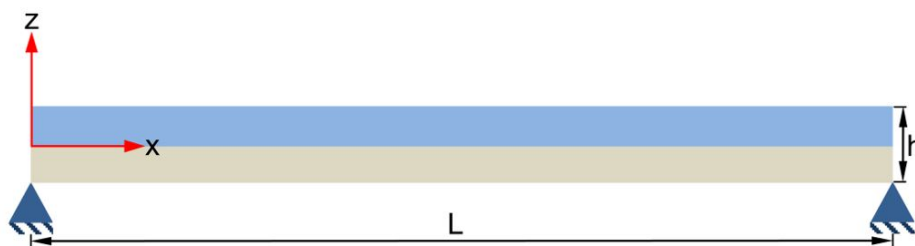


Figure 2. The coordinates and geometry of the FG beam

components of any point in the x-axis, y-axis, and z-axis, are designed by U , V , and W , respectively, Eqs. (5)-(7). The displacements for TBT and higher order shear deformation theory (HOSDT) are expressed as [33]:

$$U(x, z, t) = u(x, t) - zw(x, t) + f(z)u_1(x, t), \tag{5}$$

$$V(x, z, t) = 0, \tag{6}$$

$$W(x, z, t) = w(x, t). \tag{7}$$

$u(x, t)$ and $w(x, t)$ are the axial and transverse displacements for each location on the neutral axis. Over the thickness of a beam, the shape function $f(z)$ is used to calculate the transverse shear stress and strain distribution. The transverse shear strain on the beam centre surface has been

determined by the unknown function (u_1). As a result, $f(z)$ is equal to zero, zero, and $(4z^3/3h^2)$ in classical beam theory (CBT), first-order shear deformation beam theory (FSDBT), and HOSDT [37] FGB's normal and shear strains can be described as follows see, Eqs. (8)-(9):

$$\epsilon_{xx} = \frac{du}{dx} - \left(z \frac{d^2w}{dx^2} \right) + \left(f(z) \frac{du_1}{dx} \right), \tag{8}$$

$$\gamma_{xz} = \frac{df(z)}{dz} u_1. \tag{9}$$

The principle of minimum potential energy states that for small displacements, the variation of the total potential must be equal to zero, as shown below in Eqs. (10)-(11):

$$\delta\Pi = \delta(U_{int} - W_{ext}). \tag{10}$$

The variation in strain energy is:

$$\delta(U_{int}) = \int_0^L \left(N\delta\frac{du}{dx} - M\delta\frac{d^2w}{dx^2} + M_s\delta\frac{du_1}{dx} + Q^s\delta u_1 \right) dx. \tag{11}$$

The present study considers the applied load to be a point load (P) or distributed loads (q), as illustrated in Figure 3. The external work can be presented as:

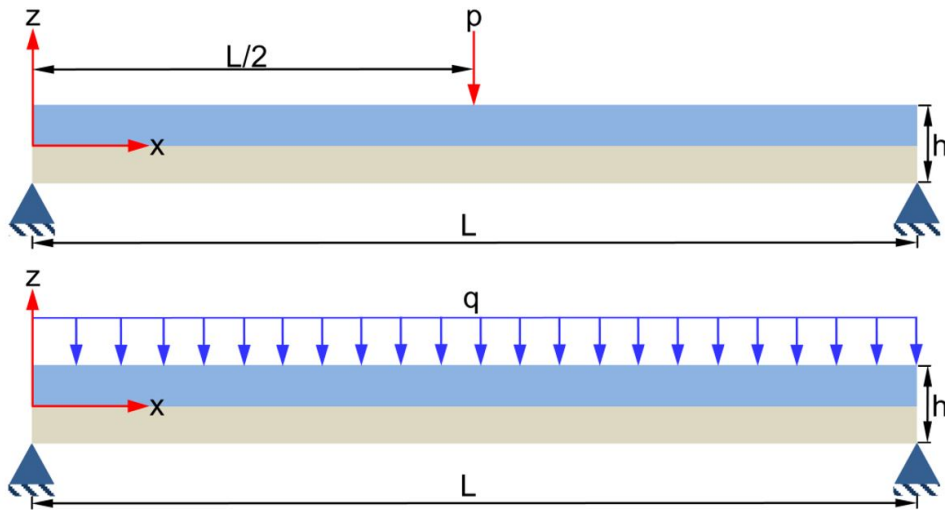


Figure 3. The applied point and distributed loads used in this study

$$\delta(W_{ext}) = \int_0^L (q_t\delta w + f_{axial}\delta u) dx, \tag{12}$$

where: q_t is the point or distributed load in the transverse direction, and f_{axial} is an axial force. According to strain energy, axial force, bending moment, and shear force are all expressed as N ,

M , M^s , and Q^s , respectively.

$$N = \int \sigma_{xx} dA, \tag{13}$$

$$M = \int z\sigma_{xx}dA, \tag{14}$$

$$M^s = \int f(z)\sigma_{xx}dA, \tag{15}$$

$$Q^s = \int \frac{df(z)}{dz}\sigma_{xz}K_s dA. \tag{16}$$

The transverse and axial loads are presented by (q) and (p) , respectively. The shear correction factor K_s can be taken as $5/6$ and 1 in Timoshenko and high-order shear deformation theories, respectively. The Eqs. (12), (13), (14), (15), and (16) can be rewritten as:

$$N = A_{11} \frac{du}{dx} - B_{11} \frac{d^2w}{dx^2} + E_{11} \frac{du_1}{dx}, \tag{17}$$

$$M = B_{11} \frac{du}{dx} - D_{11} \frac{d^2w}{dx^2} + F_{11} \frac{du_1}{dx}, \tag{18}$$

$$M^s = E_{11} \frac{du}{dx} - F_{11} \frac{d^2w}{dx^2} + H_{11} \frac{du_1}{dx}, \tag{19}$$

$$Q^s = A_{55}u_1K_s, \tag{20}$$

and

$$\begin{pmatrix} N \\ M \\ M^s \\ Q^s \end{pmatrix} = \begin{pmatrix} A_{11} & B_{11} & E_{11} & 0 \\ B_{11} & D_{11} & F_{11} & 0 \\ E_{11} & F_{11} & H_{11} & 0 \\ 0 & 0 & 0 & A_{55} \end{pmatrix} \begin{pmatrix} \frac{du}{dx} \\ -\frac{d^2w}{dx^2} \\ \frac{du_1}{dx} \\ u_1 \end{pmatrix}, \tag{21}$$

$$(A_{11}, B_{11}, D_{11}, E_{11}, F_{11}, H_{11}) = \int (E_z(1, Z, Z^2, f(z), (zf(z)), f(z)^2) dA, \tag{22}$$

$$A_{55} = \int G_z \left(\frac{df(z)}{dz} \right)^2 dA. \tag{23}$$

By substituting Eqs. (11), (12) in Eq. (10) we get:

$$\int_0^1 \left(\left(N\delta \frac{du}{dx} - M\delta \frac{d^2w}{dx^2} + M^s\delta \frac{du_1}{dx} + Q^s\delta u_1 \right) - (q_t\delta w + f_{axial}\delta u) \right) dx = 0. \quad (24)$$

By integration and putting the coefficient δu , δw , and δu_1 equal to zero, we will get:

$$-\frac{dN}{dx} - f_{axial} = 0, \quad (25)$$

$$-\frac{d^2M}{dx^2} - q_t = 0, \quad (26)$$

$$\frac{dM^s}{dx} - Q^s = 0. \quad (27)$$

In terms of displacement, the governing equations may be found by substituting the value of N , M , M^s , and Q^s from Eqs. (17)-(20), into Eqs. (25)-(27), as follows:

$$\left(A_{11} \frac{d^2u}{dx^2} \right) - \left(B_{11} \frac{d^3w}{dx^3} \right) + \left(E_{11} \frac{d^2u_1}{dx^2} \right) = 0, \quad (28)$$

$$\left(B_{11} \frac{d^3u}{dx^3} \right) - \left(D_{11} \frac{d^4w}{dx^4} \right) + \left(F_{11} \frac{d^3u_1}{dx^3} \right) + q_t = 0, \quad (29)$$

$$\left(E_{11} \frac{d^2u}{dx^2} \right) - \left(F_{11} \frac{d^3w}{dx^3} \right) + \left(H_{11} \frac{d^2u_1}{dx^2} \right) - (A_{55}K_s u_1) = 0. \quad (30)$$

For CBT, the function $f(z) = 0$, therefore, the displacements filed is:

$$U(x, z, t) = u(x, t) - z \frac{dw}{dx}, \quad (31)$$

$$V(x, z, t) = 0, \quad (32)$$

$$W(x, z, t) = w(x, t). \quad (33)$$

There is no shear effect, so the shear strain is zero. The expression of normal strain can be expressed as Eq. (34):

$$\varepsilon_{xx} = \frac{du}{dx} - \left(z \frac{d^2w}{dx^2} \right). \quad (34)$$

As with the same procedure for TBT, the values of axial force (N) and bending moment (M) in EBT are calculated using Eqs. (35)-(37)

$$N = A_{11} \frac{du}{dx} - B_{11} \frac{d^2w}{dx^2}, \quad (35)$$

$$M = B_{11} \frac{du}{dx} - D_{11} \frac{d^2w}{dx^2}, \quad (36)$$

$$\begin{bmatrix} N \\ M \end{bmatrix} = \begin{bmatrix} A_{11} & B_{11} \\ B_{11} & D_{11} \end{bmatrix} \begin{bmatrix} \frac{du}{dx} \\ -\frac{d^2w}{dx^2} \end{bmatrix}. \quad (37)$$

By substituting values of N and M in Eqs. (29) and (30), we will get the governing equations in terms of displacement as follows, Eqs. (38) and (39):

$$A_{11} \frac{d^2u}{dx^2} - B_{11} \frac{d^3w}{dx^3} = 0, \quad (38)$$

$$B_{11} \frac{d^3u}{dx^3} - D_{11} \frac{d^4w}{dx^4} + q_t = 0. \quad (39)$$

The analytical solution for deflection problem

An analytical solution to the simply supported FGB is defined using the Navier solution approach. Any point on the neutral axis has displacement functions defined as (x, t) , (w, t) , and $(u_1)(x, t)$ as products of an unknown coefficient and a trigonometric function, please see Eqs. (40)-(42) [27].

$$u(x) = \sum_{n=1}^N U_n \cos(\alpha x), \quad (40)$$

$$w(x) = \sum_{n=1}^N W_n \sin(\alpha x), \quad (41)$$

$$u_1(x) = \sum_{n=1}^N G_n \cos(\alpha x), \quad (42)$$

where U_n , W_n , and G_n are unidentified Fourier coefficients found for each value of n . Angle α can be calculated from the following Eq. (43):

$$\alpha = \frac{n\pi}{L}. \quad (43)$$

Assuming that there are no external axial loads (f), the applied load is represented by Eqs. (44) and (45) [27]

$$q(x) = \sum_{n=1}^N Q_n \sin(\alpha x), \tag{44}$$

$$Q_n = 2 \int_0^1 q(x) \sin(\alpha x) dx, \tag{45}$$

where: Q_n is the Fourier coefficient and is given for uniform or point load. The values of Q_n for uniform load (q_0) and point load (p_0) are described as follows Eqs. (46) and (47): When $q(x) = q_0$, then:

$$Q_n = 2 \int_0^1 q_0 \sin(\alpha x) dx = \frac{4q_0}{n\pi} \text{ for } n = (1, 3, 5, \dots). \tag{46}$$

And when $q(x) = p_0\delta(x - x_p)$, then:

$$Q_n = \frac{2p_0 \sin(\alpha x_p)}{l} \text{ for } n = (1, 2, 3, \dots), \tag{47}$$

where (x_p) represents the position of the point load.

Solution of first and high-order shear deformation theory

By substituting Eqs. (40), (41), (42), (45) and their derivatives in Eqs. (28)-(30) we get Eqs. (48) and (49):

$$\begin{aligned} -\alpha^2 A_{11} U_n - \alpha^3 B_{11} W_n - \alpha^2 E_{11} G_n &= 0, \\ \alpha^3 B_{11} U_n - \alpha^4 D_{11} W_n + \alpha^3 F_{11} G_n &= -Q_n, \\ -\alpha^2 E_{11} U_n - \alpha^3 F_{11} W_n - (\alpha^2 H_{11} - A_{55} K_s) G_n &= 0. \end{aligned} \tag{48}$$

By multiplying the above equation by (-1) it turns to:

$$\begin{aligned} \alpha^2 A_{11} U_n - \alpha^3 B_{11} W_n + \alpha^2 E_{11} G_n &= 0, \\ \alpha^3 B_{11} U_n + \alpha^4 D_{11} W_n - \alpha^3 F_{11} G_n &= -Q_n, \\ -\alpha^2 E_{11} U_n - \alpha^3 F_{11} W_n - (\alpha^2 H_{11} - A_{55} K_s) G_n &= 0. \end{aligned} \tag{49}$$

By solving Eq. (49) for Timoshenko and higher order shear deformation theory, Fourier coefficients (U_n, W_n, G_n) can be determined as follows:

$$\begin{aligned} U_n &= Q_n \alpha^3 ((\alpha^2 H_{11} B_{11}) + (A_{55} K_s B_{11}) - (F_{11} E_{11} \alpha^2)) / \alpha^6 ((\alpha^2 H_{11} A_{11} D_{11}) \\ &+ (A_{55} K_s A_{11} D_{11}) - (\alpha^2 A_{11} F_{11}^2) - (\alpha^2 H_{11} B_{11}^2)) \\ &- (A_{55} K_s B_{11}^2) + (2F_{11} E_{11} B_{11} \alpha^2) - (D_{11} E_{11}^2 \alpha^2), \end{aligned} \tag{50}$$

$$\begin{aligned}
W_n = & Q_n \alpha^2 ((\alpha^2 H_{11} B_{11}) + (A_{55} K_s B_{11}) - (E_{11} \alpha^2)) / \alpha^6 ((\alpha^2 H_{11} A_{11} D_{11}) \\
& + (A_{55} K_s A_{11} D_{11}) - (\alpha^2 A_{11} F_{11}^2) - (\alpha^2 H_{11} B_{11}^2) \\
& - (A_{55} K_s B_{11}^2) + (2 F_{11} E_{11} B_{11} \alpha^2) - (D_{11} E_{11}^2 \alpha^2)),
\end{aligned} \tag{51}$$

$$\begin{aligned}
G_n = & Q_n \alpha^5 ((F_{11} A_{11}) - (B_{11} E_{11})) / \alpha^6 ((\alpha^2 H_{11} A_{11} D_{11}) \\
& + (A_{55} K_s A_{11} D_{11}) - (\alpha^2 A_{11} F_{11}^2) - (\alpha^2 H_{11} B_{11}^2) \\
& - (A_{55} K_s B_{11}^2) + (2 F_{11} E_{11} B_{11} \alpha^2) - (D_{11} E_{11}^2 \alpha^2)).
\end{aligned} \tag{52}$$

Solution of Euler-Bernoulli beam theory

Using the same procedure, substituting Eqs. (40)-(42) and their derivatives into Eqs. (28) and (29) leads to the following algebraic equations:

$$A_{11}(-\alpha^2 U_n \cos(\alpha x)) - B_{11}(-\alpha^3 W_n \cos(\alpha x)) = 0, \tag{53}$$

$$B_{11}(\alpha^3 U_n \sin(\alpha x)) - D_{11}(-\alpha^4 W_n \sin(\alpha x)) + Q_n = 0. \tag{54}$$

Taking the Eqs. (53) and (54) and multiplying them by (-1) gives us the matrix below:

$$\begin{bmatrix} \alpha^2 A_{11} & -\alpha^3 B_{11} \\ -\alpha^2 B_{11} & \alpha^2 D_{11} \end{bmatrix} \begin{bmatrix} U_n \\ W_n \end{bmatrix} = \begin{bmatrix} 0 \\ Q_n \end{bmatrix}. \tag{55}$$

The Fourier coefficient (U_n, W_n) for Euler beam theory can be calculated by solving the above Eq. (55) to get Eqs. (56) and (57):

$$U_n = (Q_n B_{11}) / \alpha^3 ((A_{11} D_{11}) - B_{11}^2), \tag{56}$$

$$W_n = (Q_n A_{11}) / \alpha^4 ((A_{11} D_{11}) - B_{11}^2). \tag{57}$$

Numerical modeling

ANSYS APDL software is used to create a 2D model of the FGB in this section. A rectangular beam with dimensions length (L) and width (b) is modelled by drawing a rectangle with dimensions length (L) and width (b) (i.e. FG beam top view). A power-law model (see Eq. (1)) can be used to describe the mechanical properties of FGB as they vary along the thickness direction. This variation of material properties is simulated in ANSYS using the 281 SHELL element, which divides the thickness of the FG beam into ten layers and this means there are 11 points along the thickness of the FG beam. The material properties of each point are estimated using a power-law equation, while the material properties of each layer are the average value of two neighbouring points. To represent each layer's thickness and material properties in Figure 4, we use the "section" command after completing the two-dimensional drawing and entering the material properties of the ten layers. A mid-span point load is applied, and a distributed load is applied in the second type [38]. SHELL281 can be used to analyze thin to moderately thick shell structures. At each node, there are six degrees of freedom: translation in the axes of x , y , and z , as well as rotation about those axes. Membrane elements can only be translated if the membrane option is selected. Linear, huge rotational, and/or nonlinear applications involving tremendous strain are well suited for

shell281. Nonlinear analyses take into account changes in shell thickness. A distributed pressure is accounted for in SHELL281 by including follower (load stiffness) effects. Composite shells or sandwich constructions can be modified using SHELL281. Elements and nodes are numbered from 3250 to 9300 and 10500 to 30000, respectively.

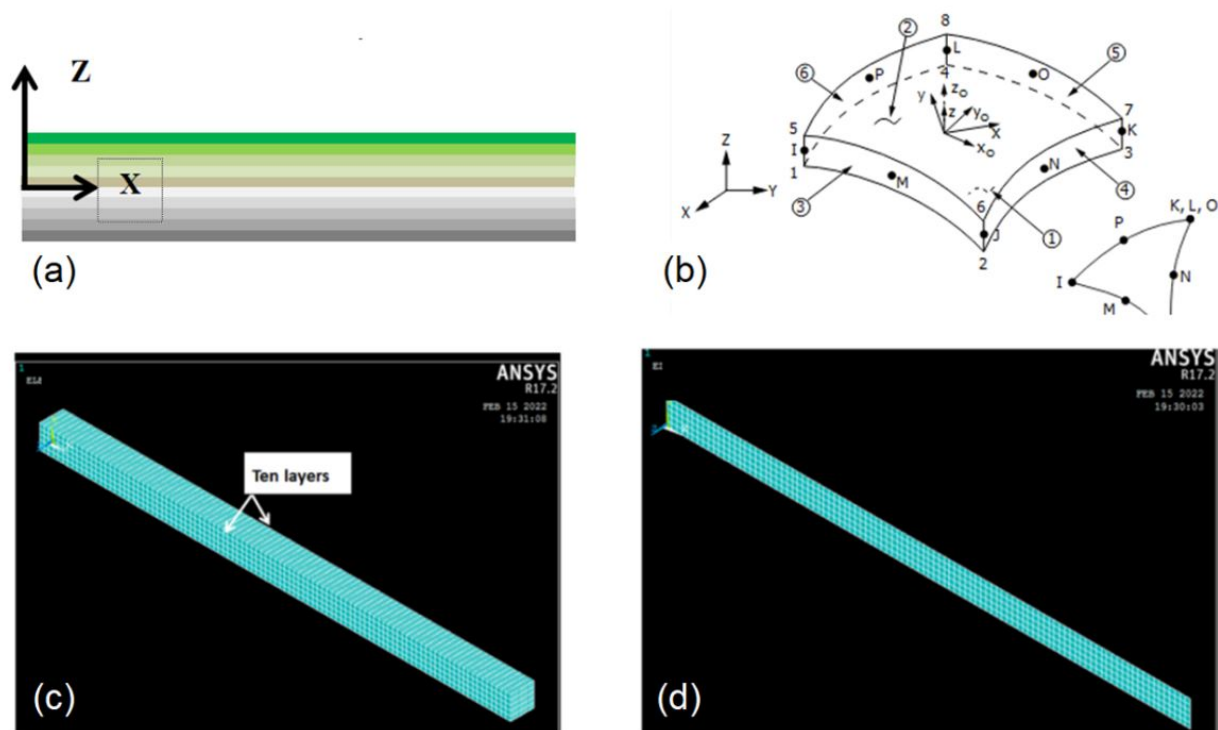


Figure 4. Drawing and Meshing of FGB, (a) ten layers arrangement, (b) element geometry, (c) meshing of FG beam, and (d) FG beam with extrude

3 Validation with previous works

In order to check the validity of the analytical and numerical models of simply supported FGB, the models are compared with the available literature.

Validation with previous work of FGB under point load

Considering a simply supported FGB, under point load p_0 , and the top surface is alumina, while the bottom surface is metal as [39, 40]:

- a. Bottom material is Aluminium: $E_{bottom} = 70 \text{ GPa}$; $\rho_{bottom} = 2700 \text{ kg/m}^3$; $\nu_{bottom} = 0.23$.
- b. Top material is Alumina: $E_{top} = 380 \text{ GPa}$; $\rho_{top} = 3800 \text{ kg/m}^3$; $\nu_{top} = 0.23$. The FG beam's dimensionless transverse deflection can be calculated using the equation below Eq. (58) [39, 40]:

$$W' = \frac{1000WE_{bottom}I}{p_0L^3}. \tag{58}$$

The dimensionless static transverse deflection of the current work is compared with Rahmani et al. [40], and the formula of Simsek and Yurtcu [27]. Table 1 shows the comparison of dimensionless transverse deflections of simply supported FG beams under point load for different power-law index ($k = 0.2, 1, 2, \text{ and } 5$) when the aspect ratio (L/h) is 5, using the presents models (CBT, TBT, HOSDT and FEM) and with previous works (Rahmani et al. [40] and Simsek and Yurtcu [27]).

While Table 2 lists the dimensionless transverse deflection of a simply supported FG beam under a point load for different models and different power-law indices when the AR is 20, comparing Rahmani et al. [40] and Simsek and Yurtcu [27].

Table 1. Verification of dimensionless transverse static deflections of simply supported FGB when the value of L/h is 5 under point load

Authors	Index value (K)			
	0.2	1	2	5
Present work CBT	4.6219	7.6025	9.7429	11.5208
Present work TBT	5.1049	8.2089	10.4776	12.595
Present work HOSDT	4.956	7.6496	9.9861	13.6018
Present work ANSYS	5.1307	7.8914	9.9738	12.771
CBT [40]	4.659	7.692	9.873	11.702
FSDBT [40]	5.18	8.434	10.889	13.373
HSDBT [40]	5.199	8.486	10.953	13.416
New Method [40]	5.185	8.466	10.832	13.41
EBT [27]	4.6219	7.6025	9.7428	11.5208
TBT [27]	5.0946	8.2923	10.6383	12.7965

Table 2. Verification of dimensionless transverse static deflections of simply supported FGB when the value of L/h is 20 under point load

Authors	Index value (K)			
	0.2	1	2	5
Present work CBT	4.6219	7.6025	9.743	11.521
Present work TBT	4.6514	7.6569	9.824	11.629
Present work HOSDT	4.6425	7.6304	9.778	11.563
Present work ANSYS	4.9045	7.6267	9.176	11.407
CBT [40]	4.66	7.692	9.873	11.702
FSDBT [40]	4.55	7.28	9.376	11.292
HSDBT [40]	4.706	7.76	9.965	11.843
New Method [40]	4.704	7.757	9.961	11.837
EBT [27]	4.6219	7.6025	9.743	11.521
TBT [27]	4.6515	7.6456	9.799	11.601

From Table 1 and Table 2, the following points can be found: For CBT, the present model is compatible with that of Simsek and Yurtcu [27], and both are close to the model of Rahmani et al. [40]. The maximum discrepancy percentage is (1.5 %) for all L/h when the index is equal to five. In TBT, when L/h is 5, the maximum percentages of discrepancy for the present model and Simsek and Yurtcu [27] compared with Rahmani et al. [40] are (5.8 and 4.3) % respectively when the index value is 5. While the maximum percentages of discrepancy for the present model and Simsek and Yurtcu [27] compared with Rahmani et al. [40] are (-2.22 and -2.23) % respectively when L/h is 20. For HOSDT when L/h is 5, the maximum percentages of discrepancy between the present model and Rahmani et al. [40] and the new method of Rahmani et al. [40] are (1.7 and 1.4) % respectively. While the maximum percentages of discrepancy between the present model and Rahmani et al. [40] and the new method of Rahmani et al. [40] are (2.37 and 2.31) % respectively, when the length to thickness ratio is 20. For the ANSYS model, the maximum percentages of discrepancy compared with CBT, FSDBT, HSDBT and the new method of Rahmani et al. [40] are

(-10.12, 6.4, 8.9 and 7.75) % when the length to thickness ratio is 5 and power index is (0.2, 1, 2 and 5) respectively. While the maximum discrepancy percentages of this model compared with CBT, FSDBT, HSDBT and the new method of Rahmani et.al. [40] are (-5.2, -4.76, 7.91, and 3)% when L/h is 20 and power index is (0.2, 1, 2 and 5) respectively.

Verification of transverse static deflection of FGB under uniform distributed load

Secondly, under a distributed load of q_0 , the characteristics of the material Al/Al₂O₃ at the bottom and top surfaces of the S-S FGB [41]:

- Bottom material is Aluminium: $E_{bottom} = 70 \text{ GPa}$; $\rho_{bottom} = 2702 \text{ kg/m}^3$; $\nu_{bottom} = 0.23$.
- Top material is Alumina: $E_{top} = 380 \text{ GPa}$; $\rho_{top} = 3960 \text{ kg/m}^3$; $\nu_{top} = 0.23$. The dimensionless static transverse deflection of the FGB as Eq. (59) [41]:

$$W' = \frac{100WE_b I}{q_0 L^4}. \quad (59)$$

The dimensionless static transverse deflections of the current study are compared to those of Farhatnia and Sarami [41], Thai and Vo [42], and Simsek and Yurtcu [27] in Table 3 and Table 4 for simply supported FGB under distributed load at different index values and length to thickness ratios. Table 3 shows dimensionless transverse deflection results for six values of power index and four models (CBT, TBT, HOSDT and ANSYS) when L/h=5 compared with available literature. While Table 4 shows the comparison among the dimensionless transverse deflections estimated by present models (CBT, TBT, HOSDT and ANSYS) with available literature for different power-law indices when L/h=20.

Table 3. Verification of dimensionless transverse static deflections of simply supported FGB when the value of L/h is 5 under distribution load

Authors	Index value (K)					
	0	0.5	1	2	5	10
Present work CBT	2.877	4.438	5.772	7.397	8.748	9.604
Present work TBT	3.161	4.764	6.168	7.916	9.429	10.42
Present work HOSDT	2.896	4.466	5.805	7.736	8.804	11.488
Present work ANSYS	3.152	4.622	5.502	7.243	8.620	9.942
CBT [42]	2.878	4.440	5.774	7.400	8.751	9.607
TBT [42]	3.165	4.828	6.259	8.067	9.828	10.938
RZT [41]	3.142	4.832	6.331	8.289	10.321	11.594
EBT [27]	2.877	4.438	5.772	7.39793	8.748	9.604
TBT [27]	3.15	4.821	6.243	8.00873	9.618	10.682

From Table 3 and Table 4, the following points can be found: For CBT and any length to thickness ratio, the present model is compatible with that of Simsek and Yurtcu [27], and both are close to the model of Thai and Vo [42]. The maximum discrepancy percentage is (0.032%) at zero index value. In TBT, the greatest discrepancy percentages of current work compared to Farhatnia and Sarami (RZT) [41] are (2.33 and 0.19) % when L/h is (5 and 20), respectively. For HOSDT, the maximum discrepancy percentages of the present model compared with RZT of Farhatnia and Sarami [41] are (6.6 and 1.7) % at L/h (5 and 20) respectively. The maximum discrepancy of percentages between ANSYS and CBT, TBT of Thai and Vo [42] and RZT of Farhatnia and Sarami [41] are (6.1, 15.3, and 15.85)% and (7.5, 8.1, and 7.76)% when L/h is 5 and 20 respectively. Based on the above validations, it can be concluded that the developed analytical and numerical models

Table 4. Verification of dimensionless transverse static deflections of simply supported FGB when the value of L/h is 20 under distribution Load distribution load

Authors	Index value (K)					
	0	0.5	1	2	5	10
Present work CBT	2.8773	4.4387	5.7727	7.3979	8.748	9.604
Present work TBT	2.8947	4.4643	5.8096	7.4542	8.823	9.682
Present work HOSDT	2.8889	4.4542	5.7701	6.8387	8.349	9.558
Present work ANSYS	2.8965	4.2764	5.7701	6.8387	8.349	9.558
CBT [42]	2.8783	4.4401	5.7746	7.4003	8.751	9.607
TBT [42]	2.8962	4.4644	5.8049	7.4421	8.818	9.690
RZT [41]	2.9127	4.4588	5.7895	7.4143	8.778	9.624
EBT [27]	2.8773	4.4387	5.7727	7.3979	8.748	9.604
TBT [27]	2.8947	4.4626	5.8022	7.4361	8.802	9.671

are in excellent agreement with the presented research on point and distributed loads and can be used as benchmarks for beam design.

4 Results and discussions

In this work, analytical solutions for the transverse deflection of FG beams using Euler, Timoshenko, and higher-order shear deformation theories have been derived. The dimensionless transverse deflection is calculated and simulated numerically by using ANSYS software. The advantages of the present analytical model of the FG beam are that it is simple and can be used to analyze the static deflection behavior of the FG beam for any other material and dimensions. FG beams are mathematically and analytically modeled for maximum transverse deflections under distributed and point loads. Numerical and analytical methods are used to study how power index value (K), aspect ratio (L/h), and modulus ratio (MR) affect the results using the material properties listed in Section 2.

FEM results for a beam with different values of power law index are shown in Figure 5 and Figure 6 under point and distributed loads with numerical effects of the length-thickness ratio. These figures show an inverse relationship between dimensionless transverse deflection and L/h for different MR. For any load type, when the modulus ratio is unity, the maximum dimensionless transverse deflection is constant with increasing power-law index because the modulus of the top material is equal to that of the bottom material. But when the MR is less than unity, the maximum dimensionless transverse deflection increases with increasing power-law index because the increase of power law index leads to make the volume fraction of strong material (i.e. bottom material) decreases and this leads to an increase in the dimensionless transverse deflection. On the other hand, the dimensionless transverse deflection decreases with increasing power-law index when the MR is greater than unity because of the increasing volume fraction of strong material (i.e. top material), while the shear effect increases with increasing aspect ratio when the length of the FG beam is constant. This fact causes a decrease in the value of the dimensionless transverse deflection when the power-law index and MR remain constant. In other words, increasing the aspect ratio changes the FG beam to be a thin FG beam, and this leads to convergence of the dimensionless transverse deflection calculated by different beam theories.

Figure 7 and Figure 8 illustrate the effects of the MR on dimensionless static transverse deflections for point loads and distributed loads at different index values and 100 aspect ratios. A constant power index causes the dimensionless transverse deflection to decrease as the MR increases. The dimensionless transverse deflection varies inversely with the power index when the MR of the bottom and top materials is less than one and the bottom material's modulus is greater than that of

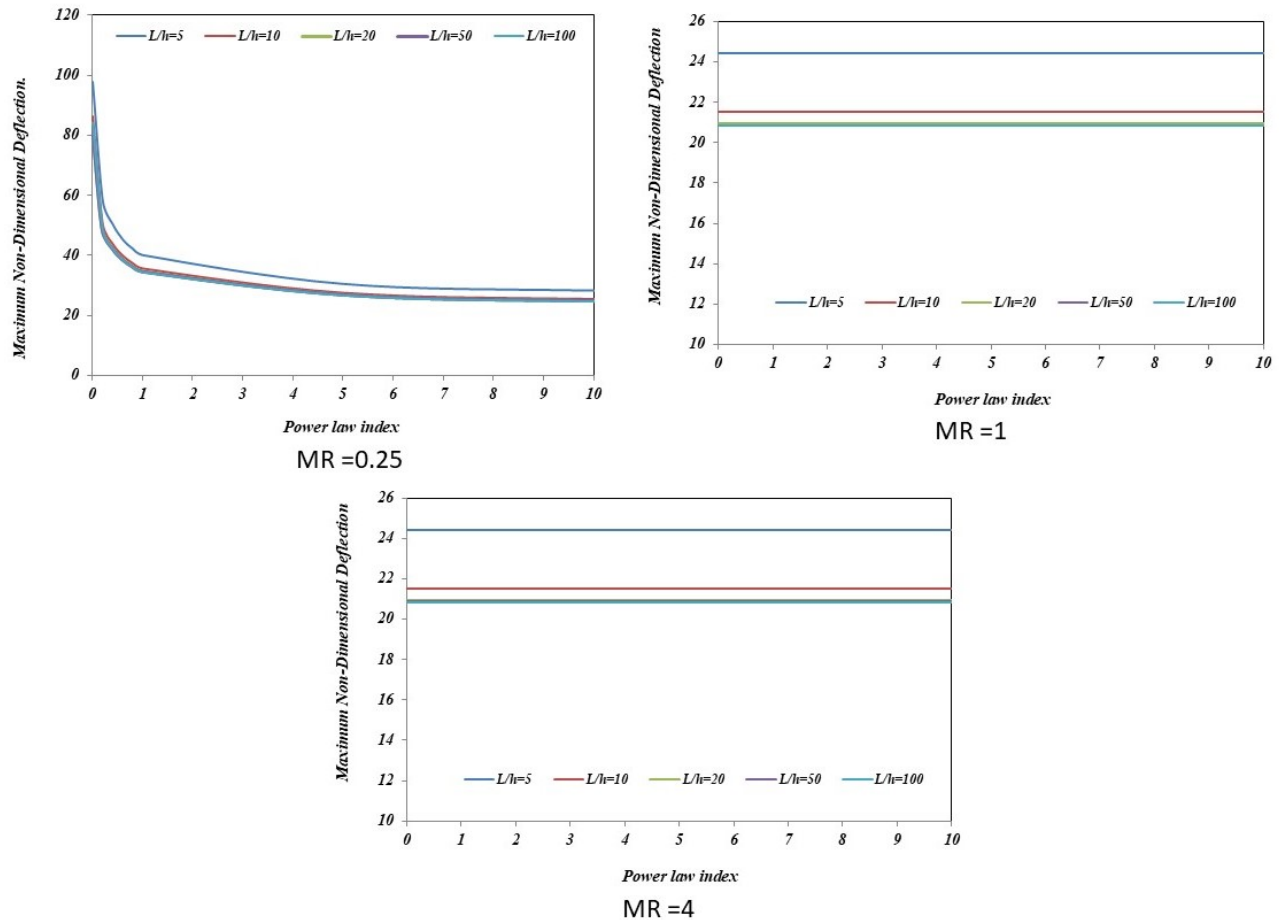


Figure 5. The dimensionless deflection of FGB under point load with different (L/h)

the top material. An MR greater than one results in a direct proportionality between dimensionless transverse deflection and the power index value for the bottom material, resulting in a lower modulus for the bottom material. Eq. (1) states that when the MR is less than one, the equivalent modulus increases directly as the power index increases, whereas when the MR is greater than one, the equivalent modulus decreases inversely. As a result, an increase in the equivalent modulus results in a decrease in the transverse deflection. Furthermore, dimensionless transverse deflections vary directly with transverse deflections. This behavior is caused by power-law-like variations in material properties. When the power-law index is zero, FG beams composed of pure ceramic (or top material) have an equivalent modulus of ceramic. As the power-law index increases, the FG beam tends to contain a mixture of metal and ceramic. The equivalent modulus is the metal modulus (or bottom material) when (i.e., a power-law index is infinity). For example, when the MR is 0.5, that means the modulus of the top material is smaller than that one in the bottom material. Therefore, the increasing value of the power index leads to an increase in the equivalent modulus of the FG beam, which subsequently decreases the maximum dimensionless transverse deflection. If the MR is 2, the modulus of the top material is larger than that of the bottom, and the equivalent modulus of the FG beam decreases with the increase in power index value so that the maximum dimensionless transverse deflection will increase. This means that the maximum power index value makes the FG beam more flexible (i.e. a pure material has a high modulus).

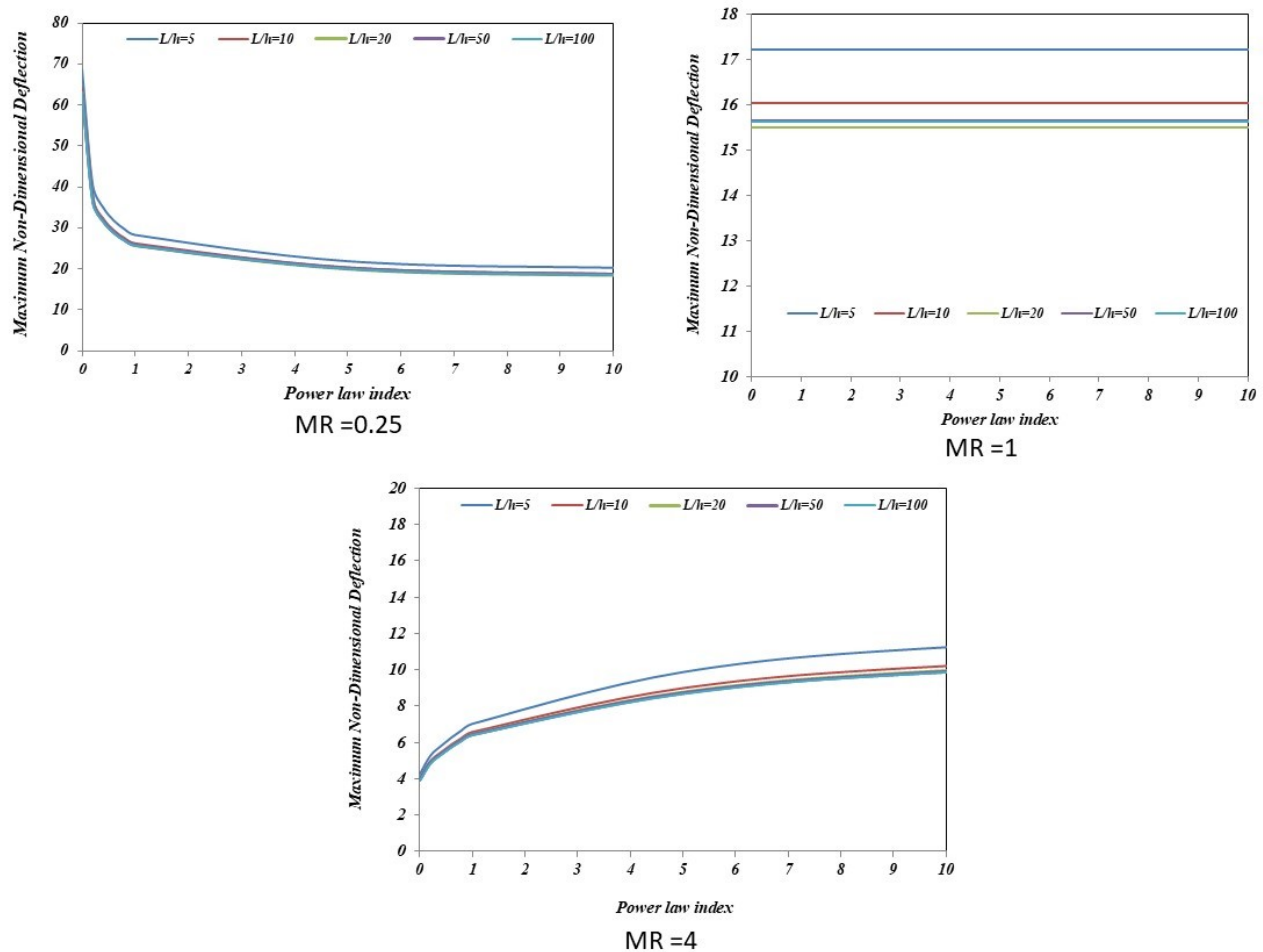


Figure 6. The dimensionless deflection of FGB under distributed load with different (L/h)

Figure 9 and **Figure 10** illustrate the effect of deformation theory on the dimensionless static transverse deflection of FGB with different values of index, MR, and different types of loads when the value of L/h is five. It can be seen from these figures that the deflection of CBT is less than that of TBT and HOSDT theories. In HOSDT, the profile of dimensionless transverse deflection variation is similar to that of CBT and TBT, but the value of this deflection is generally larger than that of CBT and TBT. This suggests that the shear effect contributes to increasing this deflection, particularly for short beams. Also, the numerical results are close to the analytical results of TBT, and results from [30] (CBT, and TBT) are close to the results of the presented model.

Figure 11 illustrates the effect of the type of loads on dimensionless deflection when the values of MR are 4 and 0.25, respectively, versus different index values and when the value of aspect ratio (L/h) is five. From the previous Figures, it can be seen that the point load has a great effect on the dimensionless deflection of FGB. A layered FG disk was fabricated using the powder metallurgy method by stacking the powder in a die in different layers [43, 44]. In a similar manner, to fabricate an FG beam, powder of the required composition is to be mixed. These powders are then stacked in a die along the die width/height. The size of the die should not be less than that of the size of the beam; some tolerances are to be provided for machining purposes. The powder is then taken to the compaction process by pressing the powder with an appropriate load to obtain a crack-free green compact. The green compact is then sintered to obtain the desired mechanical properties. The sintering temperature, compaction load and holding time vary with material to material.

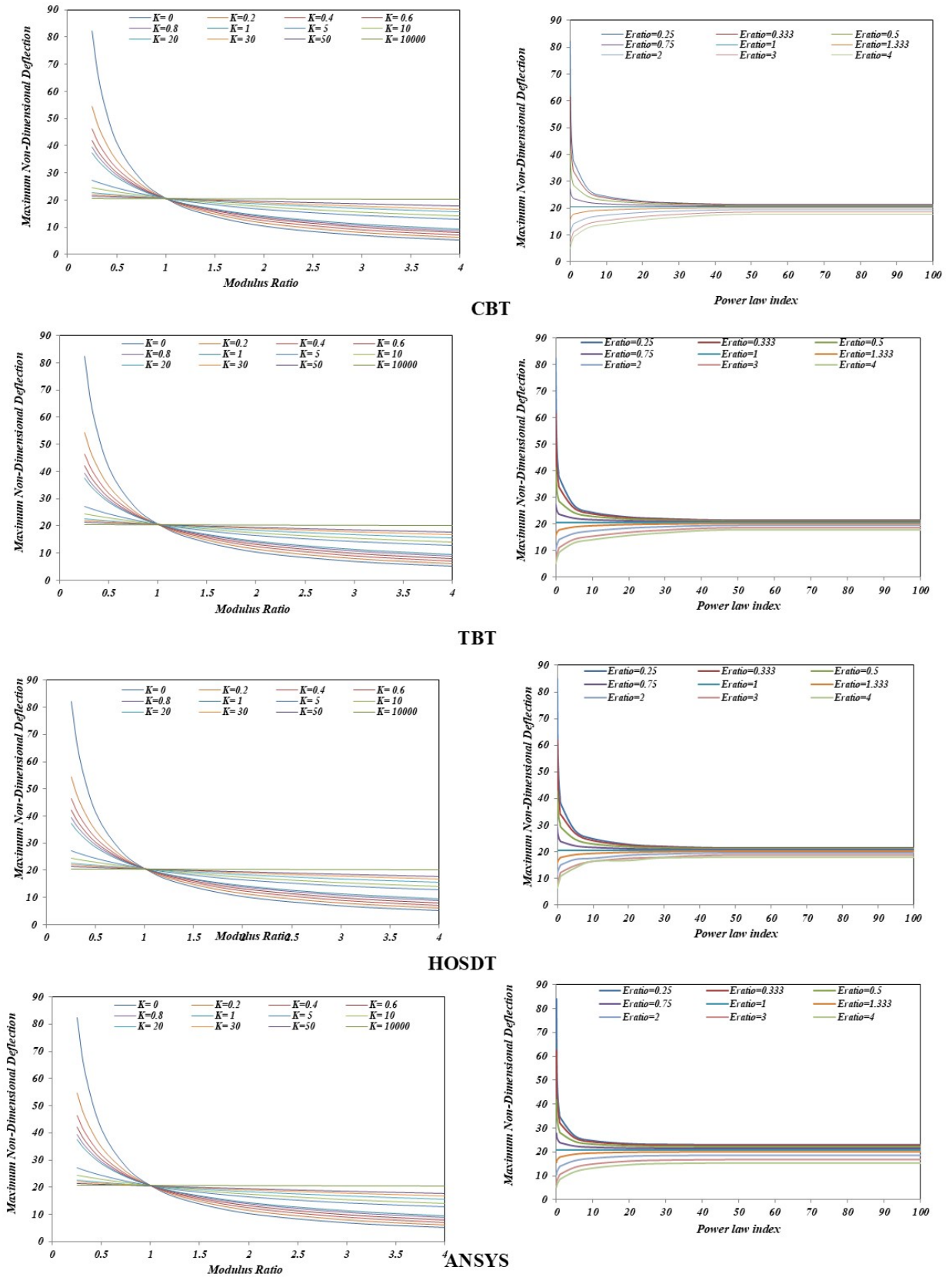


Figure 7. Effect of index value and E ratio on dimensionless deflection of FGB under point load when the L/h is 100 and for all theories

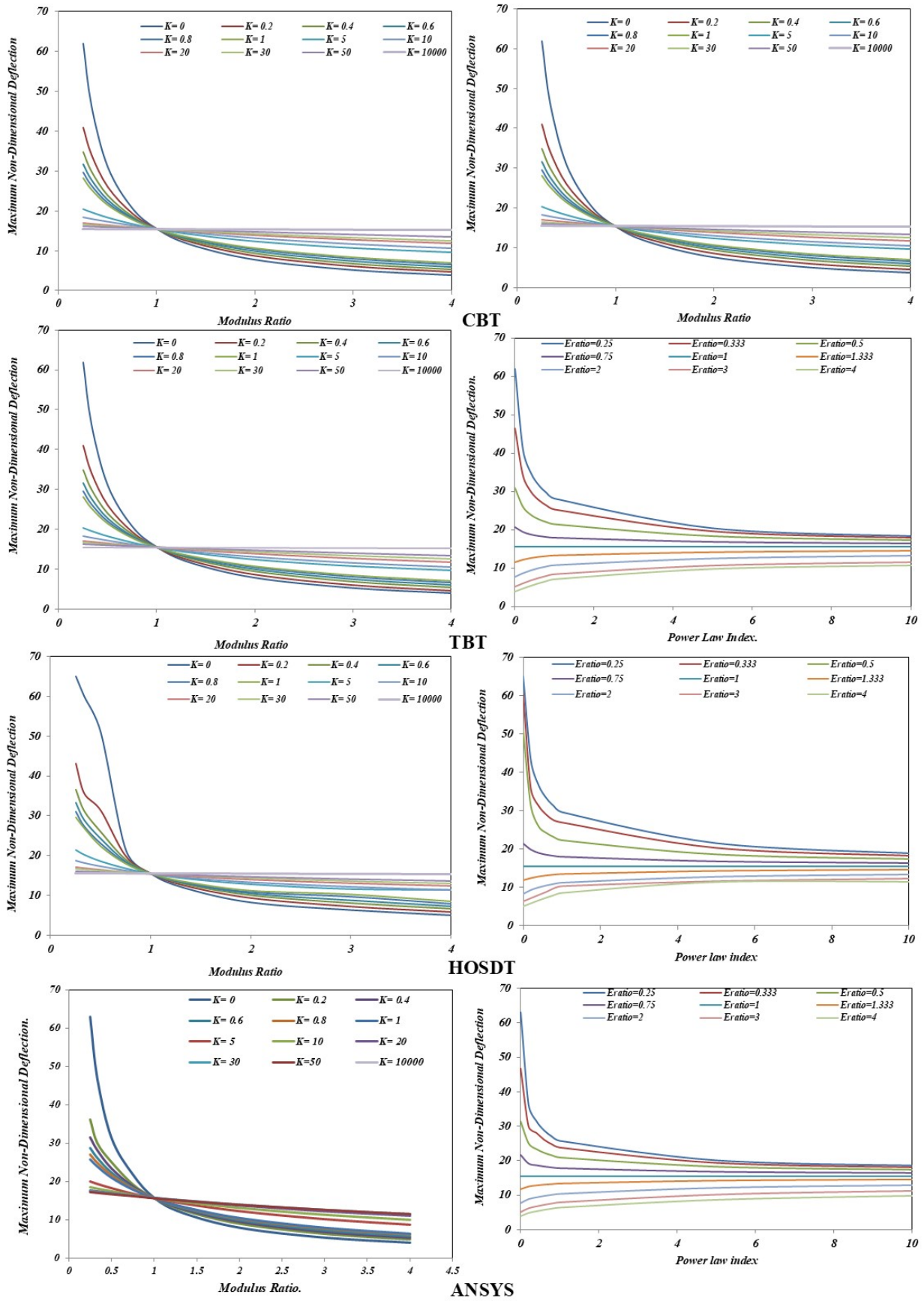


Figure 8. Effect of index value and modulus ratio on dimensionless deflection of FGB under the distributed load when L/h is 100 and for all theories

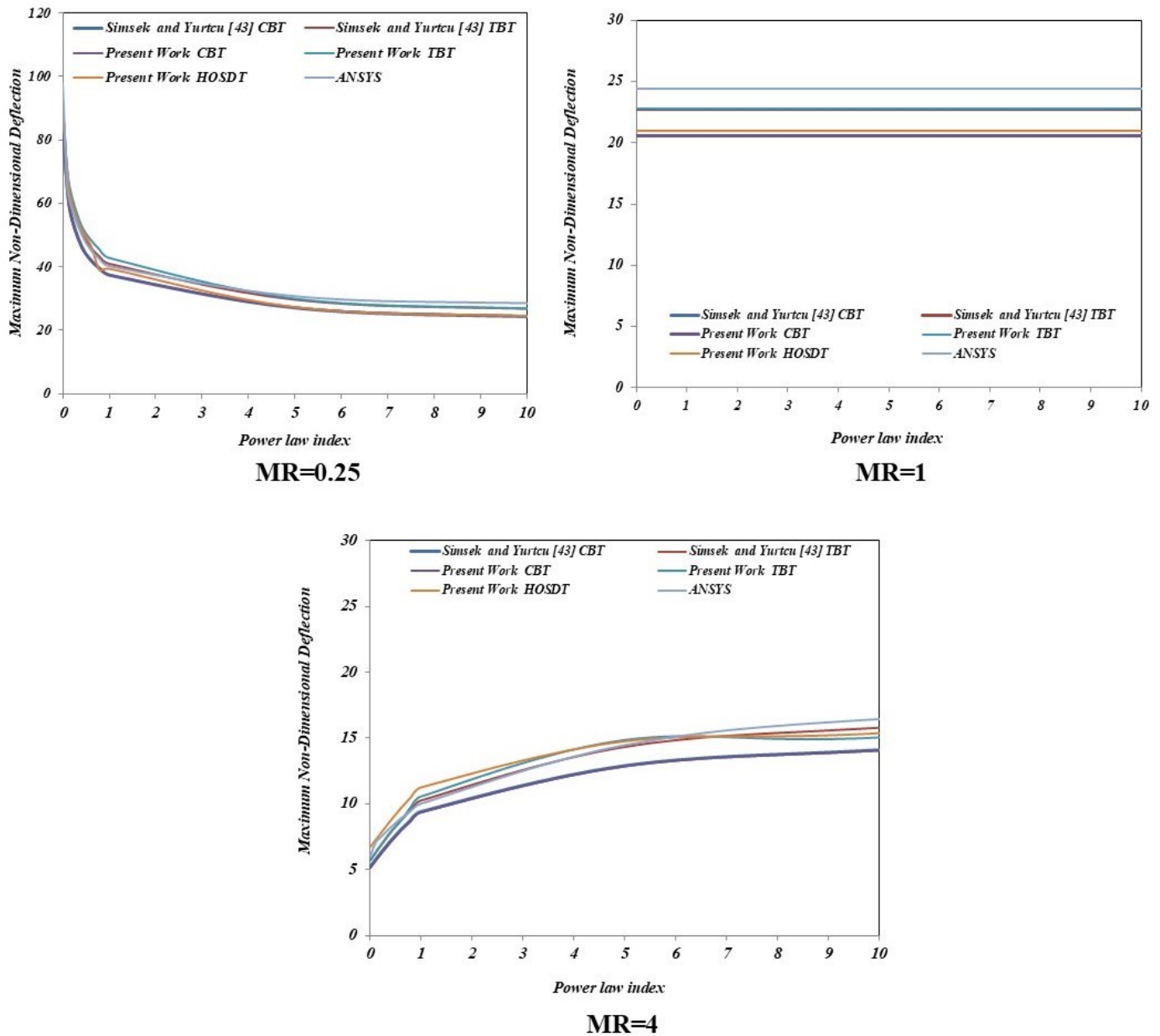


Figure 9. The effect of deformed theories on dimensionless transverse deflection of FGB under point load when the value of L/h is 5

The advantage of additive manufacturing over powder metallurgy is that, in this, as many layers can be formed, which imparts greater bonding strength and prevents delamination.

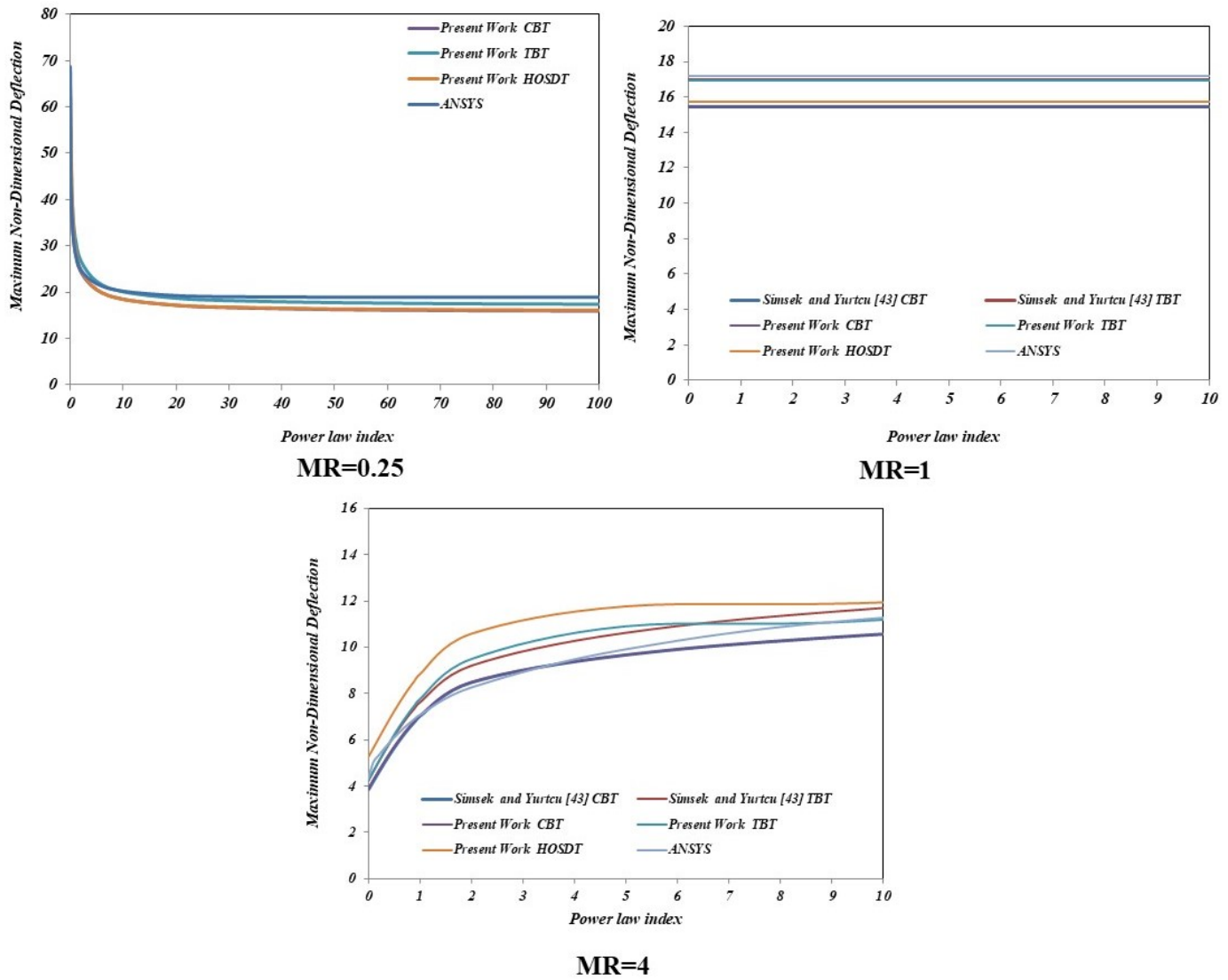


Figure 10. The effect of deformed theories on dimensionless deflection of FGB under distributed load when the L/h is 5

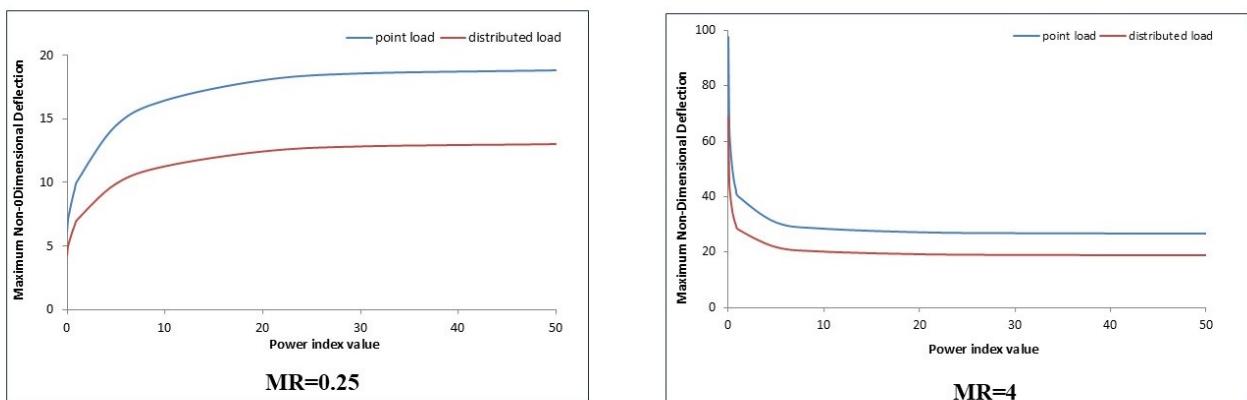


Figure 11. The effect of load type on dimensionless transverse deflection when the L/h is 5

5 Conclusions

An analytical model is constructed to perform an analysis of the static deflection of FGM beams that have been subjected to simply supported boundary conditions according to the various types of beam theory. Mechanical properties and static deflection were estimated based on two types of exerted load. Consideration is given to various parameters of modulus ratio and power-law indices. The accuracy of the new approach is simulated by using both FEM and some references found in the literature. It has been found that this technique produces satisfactory outcomes. The most important conclusions obtained from this study are listed below:

1. Index value increase leads to a decrease in and an increase in the maximum dimensionless transverse deflection when the modulus ratio is less than or greater than 1, respectively.
2. The L/h has a small effect on the behavior of FGB, but it has a great effect in each of TBT and HOSDT. This indicates that the shear significantly influences the static deflection of small beams.
3. In TBT, HOSDT, and FEM when the length-to-thickness ratio is increased, the maximum dimensionless transverse deflection is reduced.
4. The shear effect in FGB leads to an increase in the dimensionless static deflection.
5. The maximum dimensionless transverse deflection results from the TBT analytical model and numerical model are approximately identical.
6. The values of maximum dimensionless transverse deflection in the present model are in good agreement with CBT.
7. It can be seen that the present model is reliable and has the ability to calculate the static deflection for any other required beam with different loads and dimensions.

In future works, the present study can be improved to study the buckling and vibration behaviors of the FG beam. Also, the present work can be modified to study the crack effect on the static and dynamic behaviours of FG beams.

Nomenclature

Table 5. Abbreviations and their extensions

Symbol	Explanations
FGM	Functionally graded materials
TBT	Third order beam theory
FSDBT	First-order shear deformation beam theory
HSDT	Higher-order shear deformation theory
CBT	Classical plate theory
SS	Simply supported
APDL	ANSYS Parametric Design Language

Declarations

Use of AI tools

The authors declare that they have not used Artificial Intelligence (AI) tools in the creation of this article.

Data availability statement

No Data associated with the manuscript.

Ethical approval (optional)

The authors state that this research complies with ethical standards. This research does not involve either human participants or animals.

Consent for publication

Not applicable

Conflicts of interest

The authors declare that they have no conflict of interest.

Funding

No funding was received for this research.

Author's contributions

Conceptualization, R.A.H., A.A.N and E.K.N.; Methodology, R.A.H., A.A.N and E.K.N.; Software, R.A.H., A.A.N and E.K.N.; Validation, L.A, E.K.N, L.H.; Formal Analysis, L.H., A.A.N and E.K.N.; Investigation, L.A., A.A.N. and R.M.; Resources, R.A.H. and E.K.N.; Data Curation, L.H. and A.A.N, E.K.N.; Writing—Original Draft Preparation, L.H. and R.M.; Writing—Review & Editing, R.A.H, A.A.N., L.A., E.K.N. and R.M.; Visualization, E.K.N. and L.H, L.A; Supervision, E.K.N., L.H. and R.M. All authors have read and agreed to the published version of the manuscript.

Acknowledgements

The authors are grateful to the University of Kufa, College of Engineering/ Iraq, for providing facilities to carry out this work.

References

- [1] Tamrabet, A., Mourad, C., Ali Alselami, N., Menasria, A., Mamen, B. and Bouhadra, A. Efficient kinematic model for stability analysis of imperfect functionally graded sandwich plates with ceramic middle layer and varied boundary edges. *Journal of Computational Applied Mechanics*, 55(2), 184-200, (2024). [[CrossRef](#)]
- [2] Akbaş, Ş.D. Material nonlinear static analysis of axially functionally graded porous bar elements. *Journal of Computational Applied Mechanics*, 55(2), 223-234, (2024). [[CrossRef](#)]
- [3] Slimani, R., Menasria, A., Ali Rachedi, M., Mourad, C., Refrafi, S., Nimer, A.A. et al. A novel quasi-3D refined HSDT for static bending analysis of porous functionally graded Plates. *Journal of Computational Applied Mechanics*, 55(3), 519-537, (2024). [[CrossRef](#)]
- [4] Naebe, M. and Shirvanimoghaddam, K. Functionally graded materials: A review of fabrication and properties. *Applied Materials Today*, 5, 223-245, (2016). [[CrossRef](#)]
- [5] Kiarasi, F., Babaei, M., Sarvi, P., Asemi, K., Hosseini, M. and Omidi Bidgoli, M. A review on functionally graded porous structures reinforced by graphene platelets. *Journal of Computational Applied Mechanics*, 52(4), 731-750, (2021). [[CrossRef](#)]
- [6] Xu, F., Zhang, X. and Zhang, H. A review on functionally graded structures and materials for energy absorption. *Engineering Structures*, 171, 309-325, (2018). [[CrossRef](#)]
- [7] Çelik, T. and Taş, Z.C. Biomechanical evaluation of a newly developed functional-grade composite material for pedicle screws. *World Neurosurgery*, 187, e525-e533, (2024). [[CrossRef](#)]

- [8] Boggarapu, V., Gujjala, R., Ojha, S., Acharya, S., Chowdary, S. and kumar Gara, D. State of the art in functionally graded materials. *Composite Structures*, 262, 113596, (2021). [[CrossRef](#)]
- [9] Wang, X., Guo, J., Hwang, K.S. and Fang, Z.Z. Review and recent progress on developments of functionally graded WC-Co via a carburizing process: principles, insights, and industrial implications. *International Journal of Refractory Metals and Hard Materials*, 118, 106443, (2024). [[CrossRef](#)]
- [10] Ghanavati, R. and Naffakh-Moosavy, H. Additive manufacturing of functionally graded metallic materials: A review of experimental and numerical studies. *Journal of Materials Research and Technology*, 13, 1628-1664, (2021). [[CrossRef](#)]
- [11] Ansari, M., Jabari, E. and Toyserkani, E. Opportunities and challenges in additive manufacturing of functionally graded metallic materials via powder-fed laser directed energy deposition: A review. *Journal of Materials Processing Technology*, 294, 117117, (2021). [[CrossRef](#)]
- [12] Bhandari, M. and Purohit, K. Dynamic fracture analysis of functionally graded material structures—a critical review. *Composites Part C: Open Access*, 7, 100227, (2022). [[CrossRef](#)]
- [13] Sam, M., Jojith, R. and Radhika, N. Progression in manufacturing of functionally graded materials and impact of thermal treatment—A critical review. *Journal of Manufacturing Processes*, 68, 1339-1377, (2021). [[CrossRef](#)]
- [14] Kiarasi, F., Asadi, A., Babaei, M., Asemi, K. and Hosseini, M. Dynamic analysis of functionally graded carbon nanotube (FGCNT) reinforced composite beam resting on viscoelastic foundation subjected to impulsive loading. *Journal of Computational Applied Mechanics*, 53(1) 1-23, (2022). [[CrossRef](#)]
- [15] Meksi, A., Bachir Bouiadjra, R., Benyoucef, S., Bouhadra, A., Bourada, M., Ghazwani, M. and Tounsi, A. Static stability analysis of FG thick plate supported by three parameters foundation under general boundary conditions. *Journal of Computational Applied Mechanics*, 55(3), 381-400, (2024). [[CrossRef](#)]
- [16] Jin, M., Dong, X., Zhu, D., Yang, J., Lu, C., Zheng, Q. et al. Structure and properties of particles/rubber composites applied on functionally graded lapping and polishing plate. *Journal of Polymer Engineering*, 40(4), 307-313, (2020). [[CrossRef](#)]
- [17] Mellal, F., Bennai, R., Avcar, M., Nebab, M. and Atmane, H.A. On the vibration and buckling behaviors of porous FG beams resting on variable elastic foundation utilizing higher-order shear deformation theory. *Acta Mechanica*, 234, 3955-3977, (2023). [[CrossRef](#)]
- [18] Adiyaman, G. Free vibration analysis of a porous 2D functionally graded beam using a high-order shear deformation theory. *Journal of Vibration Engineering & Technologies*, 12, 2499-2516, (2024). [[CrossRef](#)]
- [19] Belkhodja, Y., Ouinas, D., Zaoui, F.Z. and Fekirini, H. An exponential-trigonometric higher order shear deformation theory (HSDT) for bending, free vibration, and buckling analysis of functionally graded materials (FGMs) plates. *Advanced Composites Letters*, 29, 1-19, (2020). [[CrossRef](#)]
- [20] Nguyen, Q.H., Nguyen, L.B., Nguyen, H.B. and Nguyen-Xuan, H. A three-variable high order shear deformation theory for isogeometric free vibration, buckling and instability analysis of FG porous plates reinforced by graphene platelets. *Composite Structures*, 245, 112321, (2020). [[CrossRef](#)]
- [21] Zhang, J., Yang, Q.S. and Liu, X. Peridynamics methodology for elasto-viscoplastic ductile fracture. *Engineering Fracture Mechanics*, 277, 108939, (2023). [[CrossRef](#)]

- [22] Akbaş, Ş.D., Fageehi, Y.A., Assie, A.E. and Eltaher, M.A. Dynamic analysis of viscoelastic functionally graded porous thick beams under pulse load. *Engineering with Computers*, 38, 365-377, (2022). [[CrossRef](#)]
- [23] Pei, Y.L. and Li, L.X. A simplified theory of FG curved beams. *European Journal of Mechanics-A/Solids*, 85, 104126, (2021). [[CrossRef](#)]
- [24] Noori, A.R., Aslan, T.A. and Temel, B. Static analysis of FG beams via complementary functions method. *European Mechanical Science*, 4(1), 1-6, (2020). [[CrossRef](#)]
- [25] Boutahar, Y., Lebaal, N. and Bassir, D. A refined theory for bending vibratory analysis of thick functionally graded beams. *Mathematics*, 9(12), 1422, (2021). [[CrossRef](#)]
- [26] Reddy, J.N., Ruocco, E., Loya, J.A. and Neves, A.M. Theories and analysis of functionally graded beams. *Applied Sciences*, 11(15), 7159, (2021). [[CrossRef](#)]
- [27] Şimşek, M. and Yurtcu, H.H. Analytical solutions for bending and buckling of functionally graded nanobeams based on the nonlocal Timoshenko beam theory. *Composite Structures*, 97, 378-386, (2013). [[CrossRef](#)]
- [28] Hadji, L., Khelifa, Z. and El Abbes, A.B. A new higher order shear deformation model for functionally graded beams. *KSCE Journal of Civil Engineering*, 20(5), 1835-1841, (2016). [[CrossRef](#)]
- [29] Chakraborty, A., Gopalakrishnan, S. and Reddy, J.N. A new beam finite element for the analysis of functionally graded materials. *International Journal of Mechanical Sciences*, 45(3), 519-539, (2003). [[CrossRef](#)]
- [30] Madan, R., Bhowmick, S., Hadji, L. and Alnujaie, A. Limit angular speed analysis of porous functionally graded rotating disk under thermo-mechanical loading. *Multidiscipline Modeling in Materials and Structures*, 19(2), 311-323, (2023). [[CrossRef](#)]
- [31] Raad, H., Najim, E.K., Jweeg, M.J., Al-Waily, M., Hadji, L. and Madan, R. Vibration analysis of sandwich plates with hybrid composite cores combining porous polymer and foam structures. *Journal of Computational Applied Mechanics*, 55(3), 485-499, (2024). [[CrossRef](#)]
- [32] Al-Furjan, M.S.H., Yin, C., Shen, X., Kolahchi, R., Zarei, M.S. and Hajmohammad, M.H. Energy absorption and vibration of smart auxetic FG porous curved conical panels resting on the frictional viscoelastic torsional substrate. *Mechanical Systems and Signal Processing*, 178, 109269, (2022). [[CrossRef](#)]
- [33] Amara, K., Bouazza, M. and Fouad, B. Postbuckling analysis of functionally graded beams using nonlinear model. *Periodica Polytechnica Mechanical Engineering*, 60(2), 121-128, (2016). [[CrossRef](#)]
- [34] Van Vinh, P. Static bending analysis of functionally graded sandwich beams using a novel mixed beam element based on first-order shear deformation theory. *Forces in Mechanics*, 4, 100039, (2021). [[CrossRef](#)]
- [35] Zhang, L., Liao, W., Fan, J. and Feng, S. A semi-analytical simulation method for bi-directional functionally graded cantilever beams under arbitrary static loads. *Smart Materials and Structures*, 33(5), 055051, (2024). [[CrossRef](#)]
- [36] Thi, T.H.N., Tran, V.K., Phung, V.M., Trinh, V.H. and Pham, Q.H. Nonlocal isogeometric analysis for bidirectional functionally graded porous curved microbeams with arbitrary boundary conditions. *Acta Mechanica Sinica*, 40, 523257, (2024). [[CrossRef](#)]
- [37] Nam, V.H., Vinh, P.V., Chinh, N.V., Thom, D.V. and Hong, T.T. A new beam model for simulation of the mechanical behaviour of variable thickness functionally graded material

beams based on modified first order shear deformation theory. *Materials*, 12(3), 404, (2019). [[CrossRef](#)]

- [38] Njim, E.K., Hasan, H.R., Jweeg, M.J., Al-Waily, M., Hameed, A.A., Youssef, A.M. and Elsayed, F.M. Mechanical properties of sandwiched construction with composite and hybrid core structure. *Advances in Polymer Technology*, 2024(1), 3803199, (2024). [[CrossRef](#)]
- [39] Madan, R. and Bhowmick, S. Fabrication, microstructural characterization and finite element analysis of functionally graded Al-Al₂O₃ disk using powder metallurgy technique. *Materials Today Communications*, 32, 103878, (2022). [[CrossRef](#)]
- [40] Rahmani, F., Kamgar, R. and Rahgozar, R. Finite element analysis of functionally graded beams using different beam theories. *Civil Engineering Journal*, 6(11), 2086-2102, (2020). [[Cross-Ref](#)]
- [41] Farhatnia, F. and Sarami, M. Finite element approach of bending and buckling analysis of FG beams based on refined zigzag theory. *Universal Journal of Mechanical Engineering*, 7(4), 147-158, (2019). [[CrossRef](#)]
- [42] Thai, H.T. and Vo, T.P. Bending and free vibration of functionally graded beams using various higher-order shear deformation beam theories. *International Journal of Mechanical Sciences*, 62(1), 57-66, (2012). [[CrossRef](#)]
- [43] Madan, R. and Bhowmick, S. Fabrication and microstructural characterization of Al-SiC based functionally graded disk. *Aircraft Engineering and Aerospace Technology*, 95(2), 292-301, (2023). [[CrossRef](#)]
- [44] Madan, R., Khobragade, P. and Bhowmick, S. Impact of porosity on free vibration and limit analysis of power-law-based functionally graded disks. *Multidiscipline Modeling in Materials and Structures*, 20(6), 1192-1212, (2024). [[CrossRef](#)]

Mathematical Modelling and Numerical Simulation with Applications (MMNSA)
(<https://dergipark.org.tr/en/pub/mmnsa>)



Copyright: © 2025 by the authors. This work is licensed under a Creative Commons Attribution 4.0 (CC BY) International License. The authors retain ownership of the copyright for their article, but they allow anyone to download, reuse, reprint, modify, distribute, and/or copy articles in MMNSA, so long as the original authors and source are credited. To see the complete license contents, please visit (<http://creativecommons.org/licenses/by/4.0/>).

How to cite this article: Neamah, R.A., Nassar, A.A., Alansari, L.S., Njim, E.K., Hadji, L. & Madan, R. (2025). Static deflection analysis of functionally graded beams using various beam theories. *Mathematical Modelling and Numerical Simulation with Applications*, 5(2), 396-420. <https://doi.org/10.53391/mmnsa.1524642>